Mitochondrial-Targeted Catalase Protects Against High-Fat Diet–Induced Muscle Insulin Resistance by Decreasing Intramuscular Lipid Accumulation

Hui-Young Lee,[1,2] Jae Sung Lee,[1] Tiago Alves,[3] Warren Ladiges,[4] Peter S. Rabinovitch,[5] Michael J. Jurczak,[3] Cheol Soo Choi,[1,2] Gerald I. Shulman,[3,6,7] and Varman T. Samuel[3,8]

Diabetes 2017;66:2072–2081 | https://doi.org/10.2337/db16-1334

We explored the role of reactive oxygen species (ROS) in the pathogenesis of muscle insulin resistance. We assessed insulin action in vivo with a hyperinsulinemic-euglycemic clamp in mice expressing a mitochondrial-targeted catalase (MCAT) that were fed regular chow (RC) or a high-fat diet (HFD) or underwent an acute infusion of a lipid emulsion. RC-fed MCAT mice were similar to littermate wild-type (WT) mice. However, HFD-fed MCAT mice were protected from diet-induced insulin resistance. In contrast, an acute lipid infusion caused muscle insulin resistance in both MCAT and WT mice. ROS production was decreased in both HFD-fed and lipid-infused MCAT mice and cannot explain the divergent response in insulin action. MCAT mice had subtly increased energy expenditure and muscle fat oxidation with decreased intramuscular diacylglycerol (DAG) accumulation, protein kinase C-θ (PKCθ) activation, and impaired insulin signaling with HFD. In contrast, the insulin resistance with the acute lipid infusion was associated with increased muscle DAG content in both WT and MCAT mice. These studies suggest that altering muscle mitochondrial ROS production does not directly alter the development of lipid-induced insulin resistance. However, the altered energy balance in HFD-fed MCAT mice protected them from DAG accumulation, PKCθ activation, and impaired muscle insulin signaling.

Muscle insulin resistance is an antecedent for the development of type 2 diabetes, but the underlying pathogenesis of impaired muscle insulin action is still debated. Some have postulated that reactive oxygen species (ROS) lead to muscle insulin resistance by altering the redox state of the muscle cell and activating redox-sensitive kinases, which in turn impair insulin signaling (1). Uncertainty exists about the role of ROS in the pathogenesis of insulin resistance. Does mitochondrial ROS production coordinate molecular signals that impair insulin action, or does it contribute to insulin resistance by promoting cumulative oxidative insults to key mitochondrial proteins that in turn impair mitochondrial function? In the latter scenario, fatty acid oxidation would be reduced, promoting accumulation of bioactive lipid intermediates (i.e., diacylglycerol [DAG]), which then would activate novel protein kinase C (nPKC) isoforms that impair muscle insulin signaling in rodents and humans (2–6).

We assessed whether a decrease in mitochondrial ROS production would protect against lipid-induced muscle insulin resistance in vivo. We studied mice overexpressing a mitochondrial-targeted catalase (MCAT) that have a decrease in mitochondrial ROS production (6,7) compared with wild-type (WT) littermates. We challenged these mice with two high-fat interventions: chronic high-fat feeding and an acute lipid infusion. MCAT mice were previously reported to be protected from diet-induced insulin resistance as a result of a decrease in ROS production (1). If ROS production primarily regulates insulin action, MCAT

[1]Department of Molecular Medicine, School of Medicine, Gachon University, Incheon, Korea
[2]Korea Mouse Metabolic Phenotyping Center, Lee Gil Ya Cancer and Diabetes Institute, Gachon University, Incheon, Korea
[3]Department of Internal Medicine, Yale University School of Medicine, New Haven, CT
[4]Department of Comparative Medicine, University of Washington, Seattle, WA
[5]Department of Pathology, University of Washington, Seattle, WA
[6]Department of Cellular and Molecular Physiology, Yale University School of Medicine, New Haven, CT
[7]Howard Hughes Medical Institute, Yale University School of Medicine, New Haven, CT
[8]Veterans Affairs Medical Center, West Haven, CT

Corresponding author: Varman T. Samuel, varman.samuel@yale.edu.

Received 31 October 2016 and accepted 30 April 2017.

This article contains Supplementary Data online at http://diabetes.diabetesjournals.org/lookup/suppl/doi:10.2337/db16-1334/-/DC1.

mice should be protected from insulin resistance in both models of lipid excess.

RESEARCH DESIGN AND METHODS

Animals

Mice overexpressing MCAT (7) were a gift from W.L. and P.S.R. Mice were housed in the animal facilities of Yale University and Gachon University. MCAT and WT mice have been backcrossed with C57BL6/NTac (Taconic) mice over five generations. The mice were individually housed under controlled temperature (23 ± 1°C) and lighting (12 h light/dark) with free access to water and fed ad libitum on regular chow (RC) (2018S; Harlan Teklad) and high-fat diet (HFD) (60% calories from fat primarily from lard and soybean oil, D12492; Research Diets, New Brunswick, NJ). For lipid infusion, mice received Liposyn II 20%, which is primarily a combination of safflower and soybean oil. All procedures were approved by the animal care and use committees of Yale University (New Haven, CT) and Gachon University (Incheon, Korea).

Body Composition and Basal Energy Balance and Hyperinsulinemic-Euglycemic Clamp Study

Body composition (lean and fat mass) was determined by ^{1}H nuclear magnetic resonance spectroscopy (MRS; BioSpin; Bruker, Billerica, MA). Basal energy balance, including oxygen consumption (VO_2), carbon dioxide production rate (VCO_2), respiratory quotient, energy expenditure, and food intake, were recorded by using a Comprehensive Laboratory Animal Monitoring System (CLAMS; Columbus Instruments, Columbus, OH) for 72 h (24 h of acclimation followed by 48 h of measurement). Three sets of hyperinsulinemic-euglycemic clamp studies were performed on overnight-fasted animals as previously described (6). Briefly, 10-week-old male mice were maintained on RC or HFD for ~6 weeks. Six to 7 days before the hyperinsulinemic-euglycemic clamp studies, indwelling catheters were placed into the right-side internal jugular vein extending to the right atrium. After an overnight fast, [3-^{3}H]glucose (high-performance liquid chromatography purified; PerkinElmer, Waltham, MA) was infused at a rate of 0.05 μCi/min for 2 h to assess the basal glucose turnover, and a hyperinsulinemic-euglycemic clamp was conducted for 140 min with continuous infusion of human insulin (3 mU/[kg-min] for RC-fed and lipid-infused mice, 4 mU/[kg-min] for HFD-fed mice; Novo Nordisk) followed by 3 min of prime infusion (~7.14 mU/[kg-min] for RC fed and lipid-infused mice, ~9.52 mU/[kg-min] for HFD-fed mice). For the acute lipid infusion study, Liposyn II (5 mL/kg/h, 20% weight for volume; Abbott Laboratories) and heparin (0.6 units/h) were infused for 4 h before insulin prime to raise plasma fatty acid concentrations. During the clamp, plasma glucose was maintained at basal concentrations (~120 mg/dL). Rates of basal and insulin-stimulated whole-body *R*d were determined by [3-^{3}H]glucose turnover during basal (0 min) and clamp steady (110–140 min) status. Tissue glucose uptake was determined by a bolus injection of 2-deoxy-D-[1-^{14}C]glucose (10 μCi/mouse; PerkinElmer) at 85 min by calculating the plasma decay of tracer activity during clamp steady status (85–140 min). The study was conducted at the Korea Mouse Metabolic Phenotyping Center (Incheon, Korea) and the National Institutes of Health-Yale Mouse Metabolic Phenotyping Center (New Haven, CT).

Mitochondria and Mouse Embryo Fibroblast Cell Isolation

Isolated skeletal muscle mitochondria were prepared as previously described with slight modifications (6). Briefly, skeletal muscles were rapidly removed and homogenized in mitochondrial isolation buffer (215 mmol/L mannitol, 75 mmol/L sucrose, 0.1% BSA, 1 mmol/L EGTA, 20 mmol/L HEPES, pH 7.2) and centrifuged at 800*g* for 10 min. The supernatant was collected and centrifuged at 10,000*g* for 10 min. Isolated mitochondria was aliquoted for measuring oxygen consumption or ROS generation. For mouse embryo fibroblast (MEF) cell isolation (4), 13–15-day postcoital mouse embryos were minced and digested with trypsin. The cells were collected and cultured in MEF medium (DMEM with 4.5 mg/L glucose, 20% FBS, 100 units/mL penicillin, and 100 μg/mL streptomycin).

ROS Measurement

Mitochondrial hydrogen peroxide (H_2O_2) generation was assessed by using 50 μmol/L Amplex red with 1 unit/mL horseradish peroxidase (Invitrogen) as described previously (8). Briefly, 100 μg of mitochondria (in 50 μL of respiration buffer) were first added to each well of a 96-well black plate (Costar 3603; Corning, Inc., Corning, NY). ROS generation was initiated by adding 50 μL of substrate (10 mmol/L succinate in the respiration buffer). Fluorescence was measured for 30 min with 2-min intervals at 37°C by using a FlexStation 3 spectrofluorometer (Molecular Devices, Sunnyvale, CA) at excitation/emission wavelengths of 550/585 nm. The value at 0 min was subtracted from the values at each time point, and H_2O_2 production rates were calculated by using a standard curve (0–10 μmol/L).

Mitochondrial Oxygen Consumption Rate and Cellular Fatty Acid Oxidation Measurement

Mitochondrial respiration and cellular fatty acid oxidation were assessed by using an XF24 analyzer (Seahorse Bioscience, North Billerica, MA) as described previously (8,9). For isolated mitochondrial respiration, 10 μg/mL mitochondria from skeletal muscle were added to the well with respiration buffer (220 mmol/L mannitol, 70 mmol/L sucrose, 10 mmol/L KH_2PO_4, 5 mmol/L $MgCl_2$, 1 mmol/L EGTA, 25 mmol/L MOPS, 0.2% BSA, pH 7.2) supplemented with oxidative substrates (10 mmol/L pyruvate, 2.5 mmol/L malate, 2.5 mmol/L glutamate, and/or 5 mmol/L succinate). All reagents were diluted in respiration buffer and loaded into the ports of the flux plate (state II–IV: port A 2 mmol/L ADP, port B 1 μg/mL oligomycin, port C 2 μmol/L carbonyl cyanide p-trifluoromethoxyphenylhydrazone, port D 2 μmol/L antimycin A). For cellular fatty acid oxidation, a 150 μmol/L palmitic acid (PA)–induced oxygen consumption rate (OCR)

was measured in Krebs-Henseleit buffer (111 mmol/L NaCl, 4.7 mmol/L KCl, 2 mmol/L $MgSO_4$, 1.2 mmol/L Na_2HPO_4, 2.5 mmol/L glucose, 0.5 mmol/L carnitine) by using the isolated MEF cells from MCAT and WT mice. The PA-induced increase in OCR was normalized to the baseline OCR (%).

Tissue Fatty Acid Oxidation Measurements

Tissue-specific fatty acid oxidation was measured by the production of $^{14}CO_2$ from [1-^{14}C]oleic acid (0.3 μCi/mL), with unlabeled oleate present in the medium as previously reported with minor modification (10). Mice were fed HFD for 6 weeks and fasted overnight. Soleus, extensor digitorum longus, and tibialis anterior muscles and liver tissue were weighed and placed in 50-mL glass flasks. The flasks had an isolated center well containing 1 N NaOH to trap $^{14}CO_2$. After 30 min of incubation at 37°C, the medium was acidified with 1 mL of 0.5 N sulfuric acid to stop the reaction. Flasks were then held at 50°C for an additional 3 h. The ^{14}C activity of the contents in the center well was counted in scintillation cocktail (Ultima Gold; PerkinElmer) by using a β-counter (Beckman Scintillation Counter; PerkinElmer).

Tissue Lipid Measurements

Membrane DAG, ceramide, and long-chain CoA (LcCoA) species were measured from gastrocnemius skeletal muscle by using liquid chromatography and tandem mass spectrometry as described previously (11), and data were expressed as the sum of individual species. Tissue triglyceride was extracted by using the method of Bligh and Dyer (12) and measured with a triglyceride reagent (Diagnostic Chemicals Ltd., Oxford, CT).

Plasma Parameters

Blood samples were taken from the tail vein after an overnight fast. Plasma nonesterified fatty acid concentrations were determined by using standard commercial kits (Wako Chemicals, Richmond, VA) according to the manufacturer's instructions. Plasma insulin levels were measured by radioimmunoassay (Linco, Billerica, MA). Plasma glucose was analyzed immediately after sampling by using the glucose oxidase method on a YSI 2700 Biochemistry Analyzer (YSI Life Sciences, Yellow Springs, OH).

Protein Extraction, Immunoprecipitation, and Western Blot Analysis

Snap-frozen gastrocnemius skeletal muscle from overnight-fasted animals was homogenized in liquid nitrogen and incubated in cell lysis radioimmunoprecipitation buffer supplemented with 1 mmol/L EDTA (pH 8.0), 10 mmol/L Tris-HCI (pH 7.4), and protease inhibitor and phosphatase inhibitor cocktails (Roche Molecular Biochemicals, Indianapolis, IN). The extracts were homogenized on ice. Samples were centrifuged for 10 min at 12,000*g*, and the supernatants were used for Western blots and immunoprecipitation. Protein concentrations were determined by Bradford assay. For phosphorylated IRS-1 protein detection, immunoprecipitation was performed. One hundred microliters of agarose A/G (BD Biosciences) were agitated for 8 h with 2 mg of total protein lysate and 2 μg of IRS-1 antibody in the cell lysis buffer at 4°C. Precipitates were washed three times with extraction buffer, and 50 μL of sample buffer was added and then boiled at 95°C for 10 min to extract the bound proteins into the supernatant. Acrylamide gel electrophoresis and transfer of separated proteins to polyvinylidene fluoride membranes were performed as previously reported (11). Immunoblots were quantified by using ImageJ software (National Institutes of Health) and normalized to GAPDH by comparing each sample with the average of WT mice. The primary antibodies used in the current study were as follows: phospho-Akt (Ser473), total Akt, phosphor-IRS-1 (Ser1101), and PTEN (Cell Signaling; Beverly, MA); protein kinase C-θ (PKCθ) and total IRS-1 (BD Biosciences); GAPDH (Santa Cruz Biotechnology, Dallas, TX); catalase (Abcam, Cambridge, MA); and β-tubulin (Millipore, Billerica, MA).

Unidirectional Rate of Muscle ATP Synthesis by In Vivo ^{31}P-MRS

After an overnight fast, the left-side hindlimb (center of gastrocnemius muscle) was positioned under a 15-mm diameter ^{31}P surface coil. The unidirectional rate of muscle ATP synthesis (V_{ATP}) was assessed by ^{31}P saturation-transfer MRS by using a 9.4-T superconducting magnet (Magnex Scientific) interfaced to a Bruker Biospec console as described previously (13).

Statistics

All values are expressed as mean ± SEM. The significance of the differences in mean values between two groups was evaluated by two-tailed unpaired Student *t* test. More than three groups were evaluated by one-way or two-way ANOVA followed by Bonferroni post hoc analysis with GraphPad Prism software. $P < 0.05$ was considered significant.

RESULTS

MCAT Mice Are Protected From Diet-Induced Muscle Insulin Resistance

Overexpression of MCAT decreased mitochondrial H_2O_2 generation by ~35% in isolated skeletal muscle mitochondria compared with WT mice (Fig. 1*A*). The reduction in ROS production did not affect insulin action in RC-fed mice: glucose infusion rate (GIR) (Fig. 1*B* and Supplementary Fig. 1*A*), insulin-stimulated whole-body R_d (Fig. 1*C*), and insulin-stimulated muscle 2-deoxyglucose uptake during hyperinsulinemic-euglycemic clamp study were identical between WT and MCAT mice (Fig. 1*D*). Hepatic insulin action was unaffected (Fig. 1*E* and *F*). On an HFD, WT and MCAT mice attained similar body weights after 6 weeks (Supplementary Fig. 2*A* and Supplementary Table 1). However, MCAT mice were protected from insulin resistance (Fig. 1*B* and Supplementary Fig. 1*B*) consistent with previous results reported by Anderson et al. (1). Specifically, MCAT mice on an HFD

had higher rates of insulin-stimulated whole-body glucose turnover (Fig. 1*C*) and gastrocnemius glucose uptake (Fig. 1*D*). Hepatic insulin action was slightly improved in the MCAT mice (Fig. 1*E* and *F*).

MCAT Overexpression Protects Against HFD-Induced Skeletal Muscle Insulin Resistance by Decreasing Intramuscular Lipid Accumulation

We sought to understand the mechanism whereby overexpression of catalase in the mitochondria protected mice from diet-induced insulin resistance. Mitochondrial ROS production remained lower in HFD-fed MCAT mice. However, mitochondrial protein carbonylation (an index of oxidative damage caused by ROS) was not different (Supplementary Fig. 2*B*). Similarly, there was no difference in the protein expression of oxidized Pten and protein tyrosine phosphatase 1B (Ptp1b) in skeletal muscle (Supplementary Fig. 2*C*), two enzymes that have been implicated in connecting ROS pathways with insulin signaling (14–16). Thus, the reduction in ROS production did not affect the oxidation of redox-sensitive proteins over the 6 weeks of high-fat feeding.

In contrast, MCAT mice had reductions in muscle lipid species, specifically intramuscular triglyceride (Fig. 2*A*), LcCoAs (Fig. 2*B*), and DAGs (Fig. 2*C*). The changes in muscle ceramide content were not significant (Supplementary Fig. 2*D*). The 60% decrease in skeletal muscle membrane DAG content (Fig. 2*C*) was associated with a decrease in PKCθ plasma membrane translocation (an index of PKC activation) (Supplementary Fig. 2*D*), an ~50% decrease in IRS-1 phosphorylation on Ser1101 (Fig. 2*E*), and an ~70% increase in insulin-stimulated AKT phosphorylation (Fig. 2*F*).

Acute Lipid Infusion Induces Skeletal Muscle Insulin Resistance in MCAT Mice Independent of Mitochondrial ROS Generation In Vivo

Acute elevations in plasma fatty acids after infusion of Liposyn and heparin induce intramyocellular lipid (IMCL) accumulation and muscle insulin resistance within several hours in rodents and humans (11,17,18). If a reduction in ROS production per se protects against lipid-induced insulin resistance, then MCAT mice should also be protected from insulin resistance after a lipid infusion. WT and MCAT mice

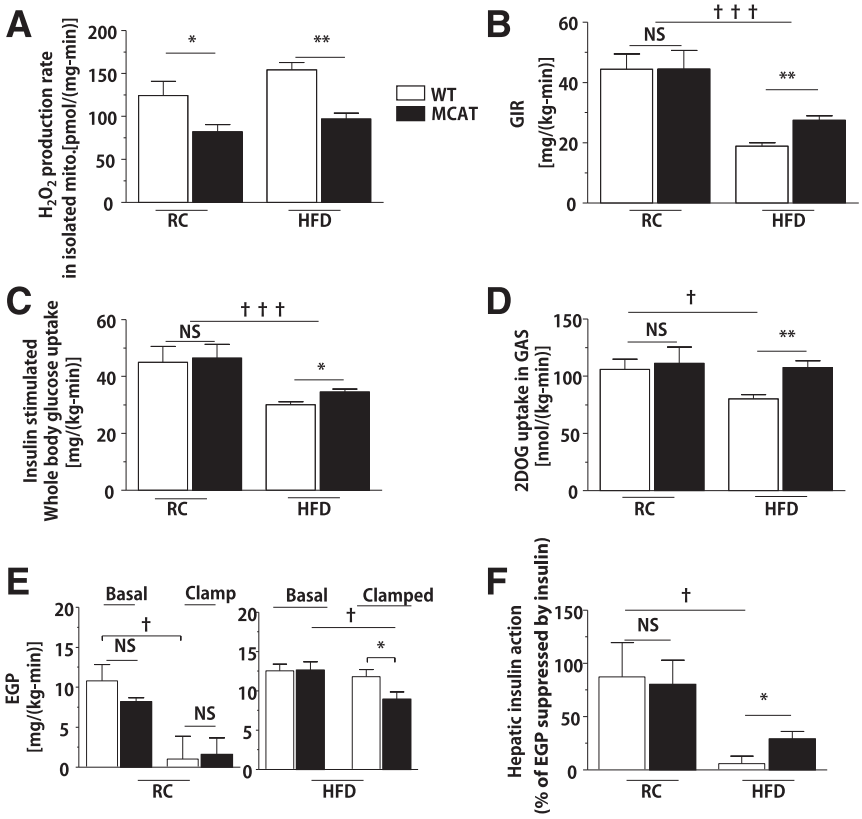

Figure 1—HFD-fed MCAT mice were protected from diet-induced muscle insulin resistance. Body weight– and age-matched MCAT and WT mice fed RC or HFD for 6 weeks and fasted overnight before hyperinsulinemic-euglycemic clamp study (RC 3 mU/[kg-min] insulin; HFD 4 mU/[kg-min] insulin). *A*: H_2O_2 production rate in isolated mitochondria from gastrocnemius (GAS) muscle of MCAT mice and littermate control (WT) mice on RC (n = 4) and HFD (n = 8–10). *B*: GIR to maintain euglycemia during hyperinsulinemic-euglycemic clamp in MCAT and WT mice on RC (n = 4) and HFD (n = 8–10). *C–E*: Insulin-stimulated peripheral R_d, insulin-stimulated muscle 2-deoxy-D-[1-^{14}C]glucose (2DOG) uptake, and endogenous glucose production (EGP) rate during the hyperinsulinemic-euglycemic clamp in MCAT and WT mice on RC (n = 4) and HFD (n = 8–10). *F*: Hepatic insulin action measured by insulin-suppressed EGP in MCAT and WT mice. Data are mean ± SEM. *P < 0.05, **P < 0.01 by Student t test; †P < 0.05, †††P < 0.001 by ANOVA. mito., mitochondria; NS, not significant.

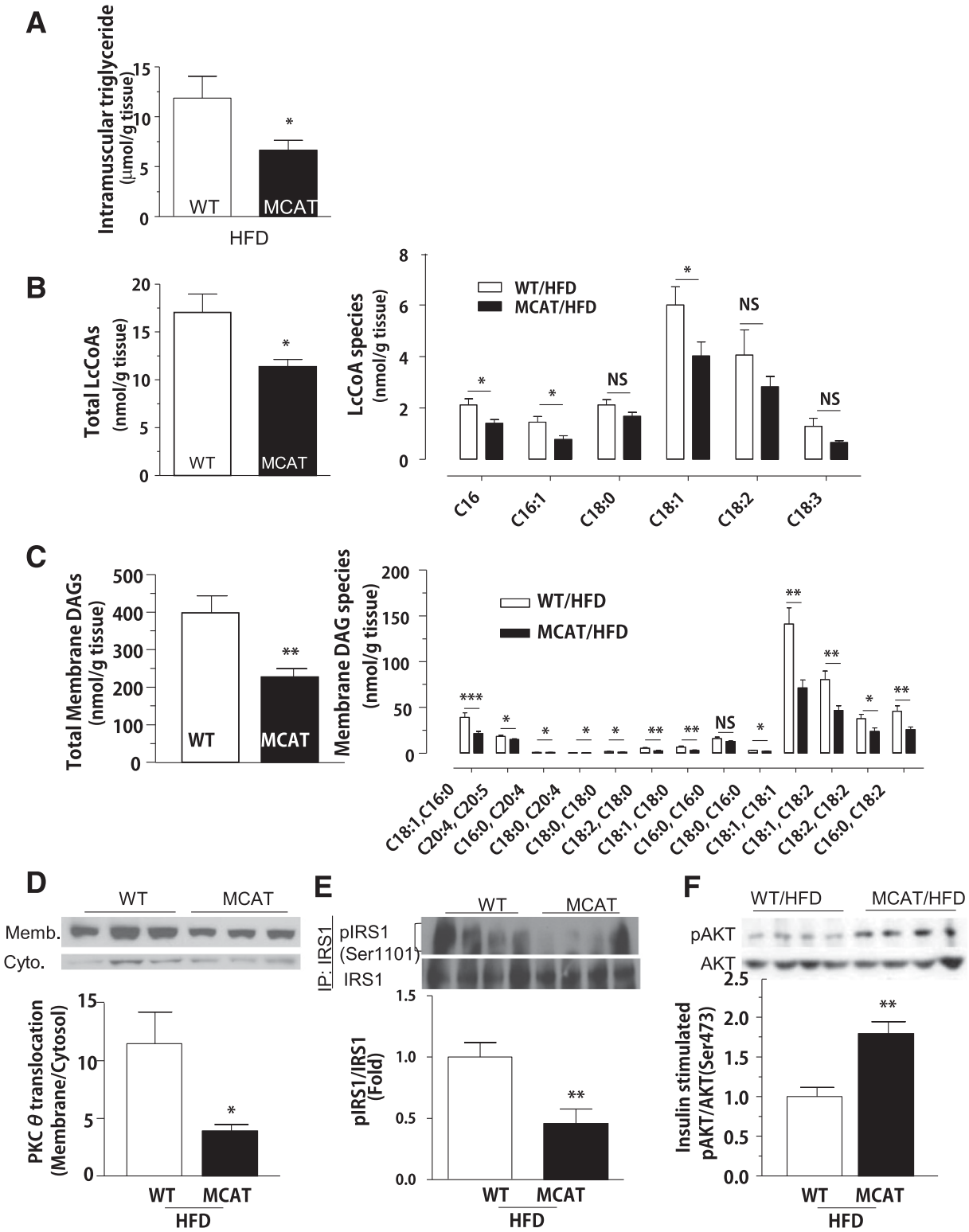

Figure 2—The protection of diet-induced muscle insulin resistance in MCAT mice is associated with decreased intramuscular lipid accumulation. Body weight– and age-matched MCAT and WT mice were fed HFD for 6 weeks and fasted 6 h before basal tissue sampling. *A–C*: Intramuscular triglyceride, total and individual LcCoA species, and total and individual DAG in gastrocnemius skeletal muscle of MCAT and WT mice. *D–F*: PKCθ membrane translocation, IRS-1 phosphorylation on Ser1101, and AKT phosphorylation on Ser473 in gastrocnemius skeletal muscle in MCAT and WT mice fed an HFD (n = 8). Data are mean ± SEM. $^*P < 0.05$, $^{**}P < 0.01$, $^{***}P < 0.001$, by Student t test. Cyto., cytosol; IP, immunoprecipitation; Memb., membrane; NS, not significant.

were infused with Liposyn + heparin for 4 h and compared with WT mice infused with saline. Liposyn infusion increased plasma fatty acid concentration by approximately threefold compared with saline infusion (Fig. 3*A*). Mitochondrial ROS generation after Liposyn infusion remained lower in skeletal muscle from MCAT mice (Fig. 3*B*) than that from WT mice. However, both WT and MCAT mice became equally insulin resistant with Liposyn infusion, as reflected by a 50% reduction in the GIR during hyperinsulinemic-euglycemic conditions (Fig. 3*C*). This decrease in insulin-stimulated whole-body glucose metabolism was attributed to a decrease in insulin-stimulated peripheral glucose uptake (Fig. 3*D*). Hepatic insulin action was not significantly changed (Fig. 3*E*) by 4-h Liposyn infusion. In a separate group of studies, WT and MCAT mice undergoing saline infusion instead of Liposyn were both equally insulin sensitive (Supplementary Fig. 4*A*–*C*). The development of insulin resistance with Liposyn infusion was associated with accumulation of intramuscular LcCoAs (Fig. 3*F* and Supplementary Fig. 4*D*) and membrane DAGs (Fig. 3*G* and Supplementary Fig. 4*F*) in both WT and MCAT mice. Muscle ceramide content was not significantly increased after Liposyn infusion (Fig. 3*H* and Supplementary Fig. 4*E*). Thus, despite the reduction in ROS production, MCAT mice subjected to an acute lipid load developed muscle DAG accumulation and muscle insulin resistance.

MCAT Overexpression Increases Mitochondrial Oxygen Consumption

We explored possibilities that may account for this divergent response to an HFD and acute lipid infusion. Body weight and body fat composition were matched between genotypes (Supplementary Fig. 3*A*). RC-fed MCAT mice showed a trend toward increased VO_2, VCO_2, and energy expenditure during a 24-h period (Supplementary Fig. 3*B*, *C*, and *E*, left panels). During HFD feeding, VO_2, VCO_2, and energy expenditure were slightly increased in the MCAT mice during the dark cycle (Supplementary Fig. 3*B*, *C*, and *E*, right panels). Of note, the total energy expenditure during the dark cycle was ~8% higher in the HFD-fed MCAT mice (211.4 ± 5.98 vs. 227.3 ± 3.87 kcal/kg; $P < 0.05$). There were no detectable differences in respiratory quotient (Supplementary Fig. 3*D*) and food intake between genotypes (Supplementary Fig. 3*F*).

Although we did not see any difference in body weight at 6 weeks of high-fat feeding, HFD-fed MCAT mice had less weight gain after 8 weeks of HFD (Fig. 4*A*), consistent with a subtle increase in energy expenditure. We quantified key parameters of myocellular energetics. Mitochondrial state III OCR (addition of ADP for ATP production) and state IV OCR (inhibition of ATPase with oligomycin) were increased in the isolated mitochondria from MCAT mice on both RC and HFD (Fig. 4*B*). Although a slight increase in state III respiration was seen, mitochondrial state IV respiration (Fig. 4*B*, right) was markedly increased in MCAT mice on HFD. Respiratory control rate calculated by the ratio of state III/IV respiration was significantly decreased in mitochondria isolated from MCAT mice on HFD (Fig. 4*C*). In addition, cellular OCR was increased in MEF cells isolated from MCAT mice compared with WT MEF cells after addition of PA as a substrate (Fig. 4*D*). These data suggest that MCAT overexpression increases mitochondrial respiration, with subtle changes in energy balance in the whole organism.

HFD-fed MCAT mice had increases in muscle lipid oxidation. Muscle tissues from MCAT mice incubated with [1-^{14}C]oleic acid produced higher amounts of $^{14}CO_2$ (Fig. 4*F*). Hepatic fatty acid oxidation was unchanged (Supplementary Fig. 1*C*). We assessed whether these alterations in mitochondrial oxygen consumption affected ATP synthesis by quantifying skeletal muscle ATP synthesis by ^{31}P-MRS. The rate of skeletal muscle V_{ATP} was identical between WT and MCAT mice (Fig. 4*G*). Similarly, cellular ATP concentration was identical between WT and MCAT MEF cells after PA treatment (Fig. 4*E*). Thus, lipid exposure increases oxygen consumption in MCAT MEFs without changing ATP synthesis.

DISCUSSION

Oxidative damage by ROS is considered an inevitable cost of aerobic biology and implicated in aging and age-associated diseases, which Harman (2) first proposed 60 years ago, postulating that ROS, such as superoxide, H_2O_2, and hydroxyl, progressively degrade biological systems, thereby decreasing cellular function and life span. Mitochondrial proteins are especially susceptible to ROS-mediated damage as reflected by declines in mitochondrial function with aging (19). For example, healthy and lean elderly individuals have an ~35% reduction in basal rates of muscle mitochondrial oxidative-phosphorylation activity (5) associated with increases in IMCL content and muscle insulin resistance. MCAT transgenic mice are protected from age-associated declines in mitochondrial function, do not accumulate ectopic lipids, and are protected from age-associated insulin resistance (6). Thus, cumulative ROS-mediated oxidative damage likely contributes to age-associated decreases in mitochondrial oxidative function.

ROS regulate a number of other cellular processes (15,16,20–24) and have been implicated in acutely regulating insulin signaling pathways distinct from their role in aging. For example, ROS are hypothesized to promote phosphatase inactivation by cysteine oxidation, thus regulating signaling pathways (23). ROS also have been implicated in enhancing insulin signaling by oxidizing and inactivating PTPs and PTEN, two proteins that dampen the insulin signaling cascade (14–16), although the major generating site of these ROS is believed to be plasma membrane–localized NADPH oxidase, not mitochondrial ROS (14–16,25). Thus, uncertainty remains about whether mitochondrial ROS production can directly affect insulin signaling and insulin sensitivity.

The data from the current studies disassociate mitochondrial ROS as a proximal cause for lipid-induced muscle

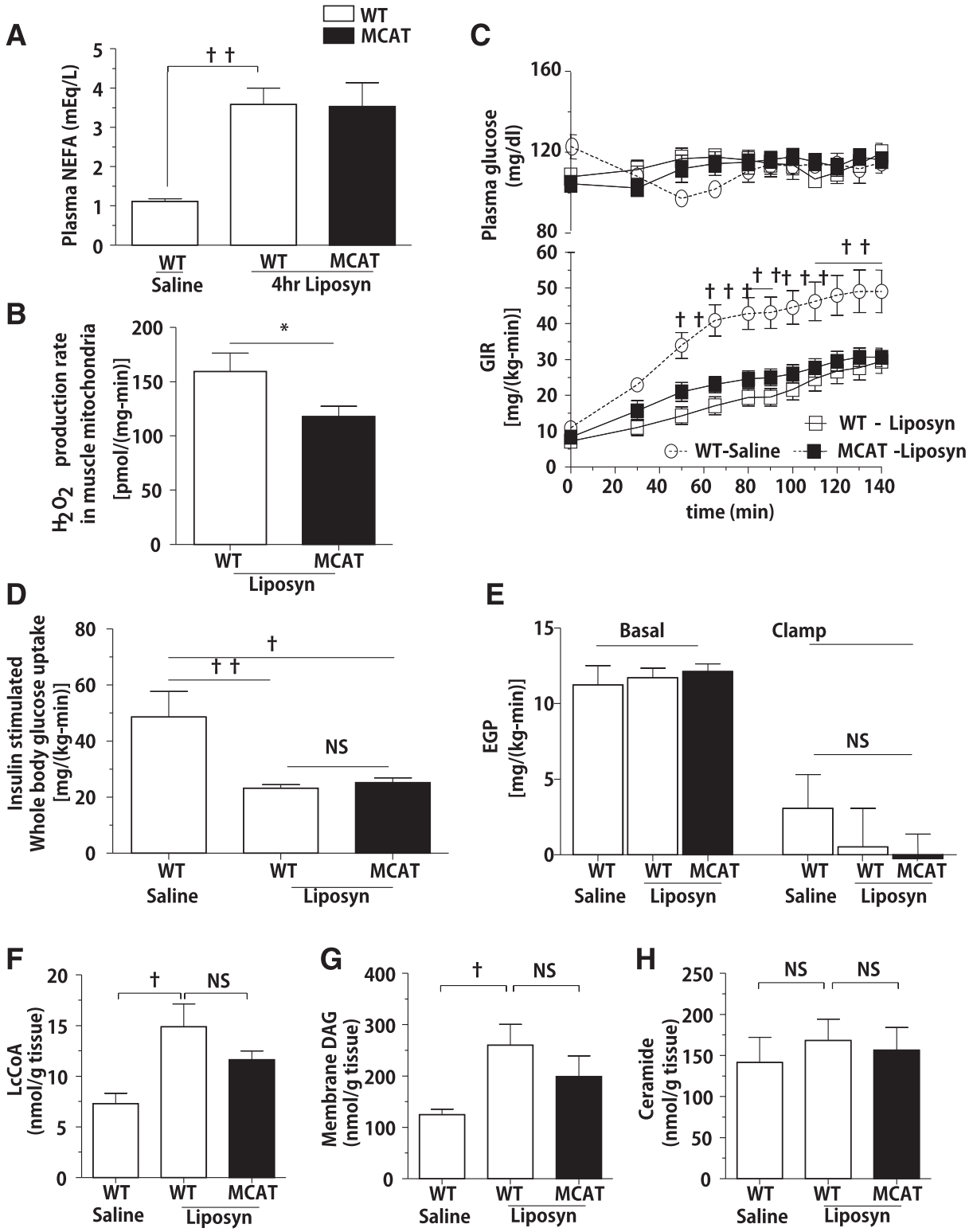

Figure 3—Acute lipid infusion induces skeletal muscle insulin in both MCAT and WT mice. Body weight– and age-matched animals were fed RC and fasted overnight before 4 h of Liposyn infusion and hyperinsulinemic-euglycemic clamp study. *A*: Plasma nonesterified fatty acid (NEFA) concentration in MCAT and WT mice after 4 h of Liposyn infusion (n = 7–8) and saline infusion (n = 4). *B*: H_2O_2 production rate in isolated mitochondria from gastrocnemius skeletal muscle of MCAT and WT mice after 4 h of Liposyn infusion (n = 7–8). *C*: Plasma glucose concentration and GIR in MCAT and WT mice to maintain euglycemia during the clamp study with 3 mU/(kg-min) insulin infusion. *D* and *E*: Insulin-stimulated peripheral R_d and endogenous glucose production (EGP) rate in MCAT and WT mice (n = 4–8) during the clamp study. *F–H*: Intramuscular LcCoAs (n = 4–8), membrane DAG (n = 4–8), and ceramide (n = 4–8) content in gastrocnemius muscle after Liposyn infusion. Data are mean ± SEM. *P < 0.05 by Student t test; †P < 0.05, ††P < 0.01, †††P < 0.001 by two-way ANOVA in *C* and by one-way ANOVA in the other panels. NS, not significant.

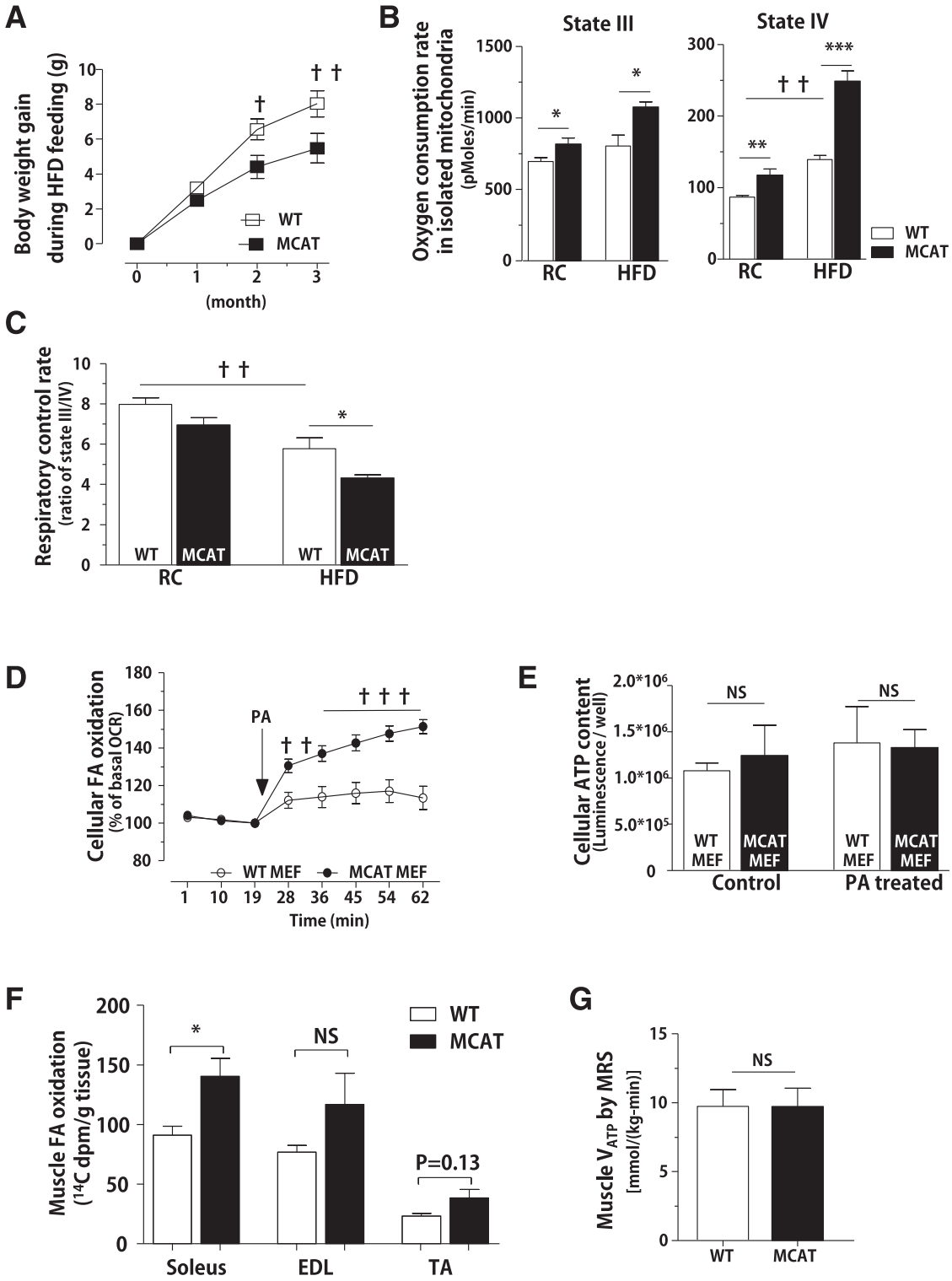

Figure 4—MCAT expression increases mitochondrial OCR without affecting ATP synthesis. Body weight– and age-matched animals fed RC or HFD for 3 months (n = 7–9). *A*: The gain of body weight in MCAT and WT mice during long-term high-fat feeding for 3 months (n = 7–9). *B*: State III and IV respiration in isolated mitochondria from WT and MCAT skeletal muscle. Mitochondria were initially energized with substrates (10 mmol/L pyruvate, 2.5 mmol/L glutamate, 2.5 mmol/L malate, 5 mmol/L succinate), and then ADP and oligomycin were added sequentially to induce state III and IV respiration, respectively. *C*: Mitochondrial respiratory control ratio. *D*: PA-induced cellular OCR measured by an XF24 analyzer. *E*: Cellular ATP content in MEF cells isolated from MCAT and WT mice (n = 3, repeated experiments). *F*: Muscle fatty acid oxidation measured by $^{14}CO_2$ production from [1-^{14}C]oleic acid in MCAT and WT mice fed HFD for 6 weeks (n = 3–4). *G*: Muscular mitochondrial V_{ATP} rate measured by ^{31}P-MRS (n = 7–8). Data are mean ± SEM. *P < 0.05, **P < 0.01, ***P < 0.001 by Student t test; †P < 0.05, ††P < 0.01, †††P < 0.001 by two-way ANOVA in *A* and *D* and by one-way ANOVA in *B* and *C*. dpm, disintegrations per minute; EDL, extensor digitorum longus; FA, fatty acid; NS, not significant; TA, tibialis anterior.

insulin resistance. As shown previously, MCAT mice were protected from HFD-induced muscle insulin resistance, which Anderson et al. (1) interpreted to support the hypothesis that the reduction in ROS production itself prevents insulin resistance. However, the current results offer an alternative cellular mechanism. First, after 6 weeks of high-fat feeding, no differences in oxidation of mitochondrial proteins (assessed by protein carbonylation) or V_{ATP} rate were found. In addition, no evidence of altered activation of oxidative-sensitive signaling pathways (e.g., PTEN, PTP1B) was observed. Instead, HFD-fed MCAT mice had decreases in IMCL content, reductions in cellular DAG concentration, and activation of PKCθ. This finding was associated with decreased serine phosphorylation of IRS-1 and improved muscle insulin signaling. Second, when these mice were challenged with an acute lipid infusion, the increases in IMCL content led to insulin resistance equivalent to littermate WT mice, despite the lower ROS production. Although ROS production was decreased in both studies, the chronic HFD and acute lipid infusion led to opposite changes in insulin action that were attributable to the changes in muscle DAG content.

The improvements in muscle insulin action in HFD-fed MCAT mice was associated with modest improvements in hepatic insulin action. In MCAT mice, we did not observe any significant alterations in hepatic fatty acid oxidation (Supplementary Fig. 1*C*), and thus, these changes could be secondary to alterations in muscle insulin action. Impairments in muscle insulin action have been associated with increased hepatic lipogenesis and can be reversed by acute bouts of exercise (26,27). The increase in hepatic lipogenesis could promote hepatic steatosis and impaired hepatic insulin action. Thus, we hypothesize that the alterations in muscle energy metabolism with MCAT overexpression may be secondarily affecting hepatic insulin action.

These studies provide additional insights into why MCAT mice were protected from HFD-induced insulin resistance. Mitochondrial content is not different in MCAT mice (6). Instead, MCAT overexpression subtly alters mitochondrial energy balance. Whole-body calorimetry demonstrated subtle increases in whole-body energy expenditure, which is consistent with increased mitochondrial OCR in RC-fed MCAT mice that was further increased by high-fat feeding. Moreover, rates of muscle fat oxidation were increased in MCAT mice, but the V_{ATP} rate was unchanged. To summarize, mitochondria in MCAT mice used more fuel to maintain ATP production. Together, these data suggest that MCAT expression promotes mitochondrial inefficiency. We note that the respiratory control rate, although higher in WT mice, also decreased with high-fat feeding in WT mice, yet these mice still developed muscle accumulation and muscle insulin resistance, which likely reflects the balance between energy intake and energy use. These changes were likely not sufficient to protect WT mice from fat accumulation over several weeks of high-fat feeding. In contrast, the subtle shift in energy balance in MCAT mice was sufficient to prevent the accumulation of excess dietary lipids and the development of insulin resistance in the muscles of MCAT mice fed an HFD over several weeks. However, the acute lipid load with a Liposyn infusion likely overwhelmed this increased oxidative capacity, leading to lipid accumulation and promoting insulin resistance. Thus, these studies highlight the primacy of energy balance and ectopic lipid accumulation as key determinants for the development of insulin resistance. Alterations in ROS production may still affect age-associated insulin resistance over the long term, but their connections to insulin resistance with increased shorter lipid exposures remains unclear. In contrast, DAG accumulation, nPKC activation, and altered muscle insulin action remain tightly associated. This pathway also provides a mechanistic link that connects mitochondrial function with the development of insulin resistance (6,17,28). The association among myocellular DAG content, nPKC activation, and insulin resistance has also been observed in humans (17,29). These studies can inform therapeutic interventions. Therapies that reduce ROS formation are unlikely to have an immediate benefit in improving insulin action. Whether long-term treatments can allay the reductions in mitochondrial function with aging is uncertain. In contrast, medications that decrease IMCL content either by shifting lipids to adipose tissue (e.g., pioglitazone [30]) or by promoting mild uncoupling have clinical utility in treating patients with insulin resistance (9,31). Additional study into the mechanisms by which MCAT induces subtle oxidation could lead to new therapies that promote subtle increases in mitochondrial substrate oxidation and prove to be viable clinical tools against the global epidemic of insulin resistance and diabetes.

Acknowledgments. The authors thank Dr. Andreas L. Birkenfeld, Dr. Dominique Pesta, Dr. Joao-Paulo G. Camporez, Dr. Francois R. Jornayvaz, Dr. Dong Zhan, Mario Kahn, Blas Guigni, Yanna Kosover, and Aida Groszmann (Yale School of Medicine) and Dr. Shi-Young Park, Dr. Kyung-Hoon Jeong, Dr. Cheol-Soon Lee, and Hyun-Jun Park (School of Medicine, Gachon University) for invaluable expert technical assistance and helpful discussion with the studies.

Funding. This work was supported by grants from the National Institute of Diabetes and Digestive and Kidney Diseases (R01-DK-40936, P30-DK-45735, U2C-DK-059635); a U.S. Department of Veterans Affairs VA Merit Award (I01 BX000901); the Ministry of Science, ICT & Future Planning (NRF-2014R1A1A1002009, NRF-2014M3A9D5A01073886, and NRF-2017R1A2B4009936); and the Korea Healthcare Technology R&D Project, Ministry for Health, Welfare & Family Affairs (HI14C1135).

Duality of Interest. No potential conflicts of interest relevant to this article were reported.

Author Contributions. H.-Y.L., C.S.C., G.I.S., and V.T.S. designed the research. H.-Y.L., J.S.L., T.A., and M.J.J. performed the research. H.-Y.L., J.S.L., G.I.S., and V.T.S. analyzed data. H.-Y.L., W.L., and P.S.R. contributed reagents. H.-Y.L., G.I.S., and V.T.S. wrote the manuscript. V.T.S. is the guarantor of this work and, as such, had full access to all the data in the study and takes responsibility for the integrity of the data and the accuracy of the data analysis.

References

1. Anderson EJ, Lustig ME, Boyle KE, et al. Mitochondrial H2O2 emission and cellular redox state link excess fat intake to insulin resistance in both rodents and humans. J Clin Invest 2009;119:573–581

2. Harman D. Aging: a theory based on free radical and radiation chemistry. J Gerontol 1956;11:298–300
3. Harman D. Free radical theory of aging: dietary implications. Am J Clin Nutr 1972;25:839–843
4. Petersen KF, Morino K, Alves TC, et al. Effect of aging on muscle mitochondrial substrate utilization in humans. Proc Natl Acad Sci U S A 2015;112:11330–11334
5. Petersen KF, Befroy D, Dufour S, et al. Mitochondrial dysfunction in the elderly: possible role in insulin resistance. Science 2003;300:1140–1142
6. Lee HY, Choi CS, Birkenfeld AL, et al. Targeted expression of catalase to mitochondria prevents age-associated reductions in mitochondrial function and insulin resistance. Cell Metab 2010;12:668–674
7. Schriner SE, Linford NJ, Martin GM, et al. Extension of murine life span by overexpression of catalase targeted to mitochondria. Science 2005;308:1909–1911
8. Zaha VG, Qi D, Su KN, et al. AMPK is critical for mitochondrial function during reperfusion after myocardial ischemia. J Mol Cell Cardiol 2016;91:104–113
9. Perry RJ, Kim T, Zhang XM, et al. Reversal of hypertriglyceridemia, fatty liver disease, and insulin resistance by a liver-targeted mitochondrial uncoupler. Cell Metab 2013;18:740–748
10. Jaworski K, Ahmadian M, Duncan RE, et al. AdPLA ablation increases lipolysis and prevents obesity induced by high-fat feeding or leptin deficiency. Nat Med 2009;15:159–168
11. Yu C, Chen Y, Cline GW, et al. Mechanism by which fatty acids inhibit insulin activation of insulin receptor substrate-1 (IRS-1)-associated phosphatidylinositol 3-kinase activity in muscle. J Biol Chem 2002;277:50230–50236
12. Bligh EG, Dyer WJ. A rapid method of total lipid extraction and purification. Can J Biochem Physiol 1959;37:911–917
13. Choi CS, Befroy DE, Codella R, et al. Paradoxical effects of increased expression of PGC-1alpha on muscle mitochondrial function and insulin-stimulated muscle glucose metabolism. Proc Natl Acad Sci U S A 2008;105:19926–19931
14. Goldstein BJ, Mahadev K, Wu X. Redox paradox: insulin action is facilitated by insulin-stimulated reactive oxygen species with multiple potential signaling targets [published correction appears in Diabetes 2005;54:1249]. Diabetes 2005;54:311–321
15. Tonks NK. Protein tyrosine phosphatases: from genes, to function, to disease. Nat Rev Mol Cell Biol 2006;7:833–846
16. Sena LA, Chandel NS. Physiological roles of mitochondrial reactive oxygen species. Mol Cell 2012;48:158–167
17. Szendroedi J, Yoshimura T, Phielix E, et al. Role of diacylglycerol activation of PKCθ in lipid-induced muscle insulin resistance in humans. Proc Natl Acad Sci U S A 2014;111:9597–9602
18. Griffin ME, Marcucci MJ, Cline GW, et al. Free fatty acid-induced insulin resistance is associated with activation of protein kinase C theta and alterations in the insulin signaling cascade. Diabetes 1999;48:1270–1274
19. Hebert SL, Lanza IR, Nair KS. Mitochondrial DNA alterations and reduced mitochondrial function in aging. Mech Ageing Dev 2010;131:451–462
20. Houstis N, Rosen ED, Lander ES. Reactive oxygen species have a causal role in multiple forms of insulin resistance. Nature 2006;440:944–948
21. Evans JL, Goldfine ID, Maddux BA, Grodsky GM. Oxidative stress and stress-activated signaling pathways: a unifying hypothesis of type 2 diabetes. Endocr Rev 2002;23:599–622
22. Veal EA, Day AM, Morgan BA. Hydrogen peroxide sensing and signaling. Mol Cell 2007;26:1–14
23. Rhee SG. Cell signaling. H2O2, a necessary evil for cell signaling. Science 2006;312:1882–1883
24. Loh K, Deng H, Fukushima A, et al. Reactive oxygen species enhance insulin sensitivity. Cell Metab 2009;10:260–272
25. Fisher AB. Redox signaling across cell membranes. Antioxid Redox Signal 2009;11:1349–1356
26. Petersen KF, Dufour S, Savage DB, et al. The role of skeletal muscle insulin resistance in the pathogenesis of the metabolic syndrome. Proc Natl Acad Sci U S A 2007;104:12587–12594
27. Rabøl R, Petersen KF, Dufour S, Flannery C, Shulman GI. Reversal of muscle insulin resistance with exercise reduces postprandial hepatic de novo lipogenesis in insulin resistant individuals. Proc Natl Acad Sci U S A 2011;108:13705–13709
28. Jang C, Oh SF, Wada S, et al. A branched-chain amino acid metabolite drives vascular fatty acid transport and causes insulin resistance. Nat Med 2016;22:421–426
29. Itani SI, Ruderman NB, Schmieder F, Boden G. Lipid-induced insulin resistance in human muscle is associated with changes in diacylglycerol, protein kinase C, and IkappaB-alpha. Diabetes 2002;51:2005–2011
30. Rasouli N, Raue U, Miles LM, et al. Pioglitazone improves insulin sensitivity through reduction in muscle lipid and redistribution of lipid into adipose tissue. Am J Physiol Endocrinol Metab 2005;288:E930–E934
31. Perry RJ, Zhang D, Zhang XM, Boyer JL, Shulman GI. Controlled-release mitochondrial protonophore reverses diabetes and steatohepatitis in rats. Science 2015;347:1253–1256